JOURNAL OF MATERIALS SCIENCE 22 (1987) 2094–2104

Interlaminar fracture morphology of carbon fibre/PEEK composites

R. A. CRICK, D. C. LEACH, P. J. MEAKIN, D. R. MOORE
Analytical and Polymer Science Group, Research and Technology Department, PO Box 90, Wilton, Middlesborough, Cleveland TS6 8JE, UK

The interlaminar fracture morphology of a carbon fibre/poly(ether–ether–ketone) composite (Aromatic Polymer Composite, APC-2) has been examined. The techniques used included scanning electron microscopy on fracture surfaces and on polished and etched sections. Two types of interlaminar fracture are observed: stable and unstable fracture. Both fracture surfaces exhibit microductility but it is more extensive for stable fracture. The fracture surfaces are not planar but have surface roughness. Fibre breakage and peeling are also observed and a quantitative examination enables the fracture energy contributions from the various processes to be calculated. The use of an etching technique reveals the spherulite texture and the presence of a deformation zone which extends into the bulk of the composite from the fracture surface. The extent of this zone is greater in the stable fracture region than in the unstable region and its presence indicates that the volume of composite which can be brought into the energy absorbing process extends well beyond the interlaminar region. The size of the zone has also been calculated using the fracture energy contributions and there is moderate agreement between calculated and observed zone size. Patterns of microductility on the fracture surface are seen to be due to spherulite texture, however the spherulite boundaries do not influence the fracture path.

1. Introduction

Continuous carbon fibre reinforced composites with various thermoplastic matrices are now available. These materials are of considerable interest in highly demanding applications such as aerospace. In comparison with thermosetting composites they show improvements in a range of properties combined with the versatility of a wide range of processing techniques [1–3]. One of the areas in which they show major improvements is in interlaminar toughness and hence resistance to delamination which has been identified as a limitation of current thermosetting composites [4, 5].

One such thermoplastic composite is Aromatic Polymer Composite-2 (APC-2) which consists of a matrix of poly(ether–ether–ketone) (PEEK) reinforced with 61 vol % of continuous, unidirectional carbon fibres. There have already been a number of evaluations of the toughness of this material including impact, damage tolerance and intrinsic toughness using fracture mechanics approaches [5–11]. A major concern in aerospace structures is resistance to delamination, but tests used to assess this are often dependent on geometry. In order to eliminate this problem, fracture mechanics approaches have been used [5, 7–11]. The propagation of cracks in various directions relative to fibres in a unidirectional composite has enabled a critical strain energy release rate (G_c) or a critical stress field intensity factor (K_c) to be determined [8, 9]*. The principal direction of interest for cracking is interlaminar in which delamination cracks are propagated. The toughness in this mode is usually assessed using a double cantilever beam (DCB) test [12], and some of these experiments are referred to further in Section 2.

Whilst linear elastic fracture mechanics theory can quantitatively analyse the forces and energies derived from these tests to give values of K_c and G_c, the limitations of the analysis are apparent when a full interpretation of the toughness values is attempted. A multiplicity of failure mechanisms can occur even when the crack is propagated in a single plane, and consequently a value of fracture toughness represents an integral of the various processes.

In order to understand the failure processes further it is usual to examine the fracture surfaces microscopically and produce a qualitative description of the fracture morphology. This can then be related to the fracture toughness measurements to give an improved interpretation of the fracture process [8, 13, 14]. Our approach has been to conduct a detailed examination of delamination fracture morphology of APC-2 using both conventional and novel microscopy techniques, and initial results of this have already been published [11]. In this work we extend these initial experiments and use the microscopy observations in a quantitative

*All fractures in this paper relate to a crack opening mode. The fracture mechanics parameters K_{IC} and G_{IC} are here abbreviated to K_c and G_c.

0022–2461/87 $03.00 + .12

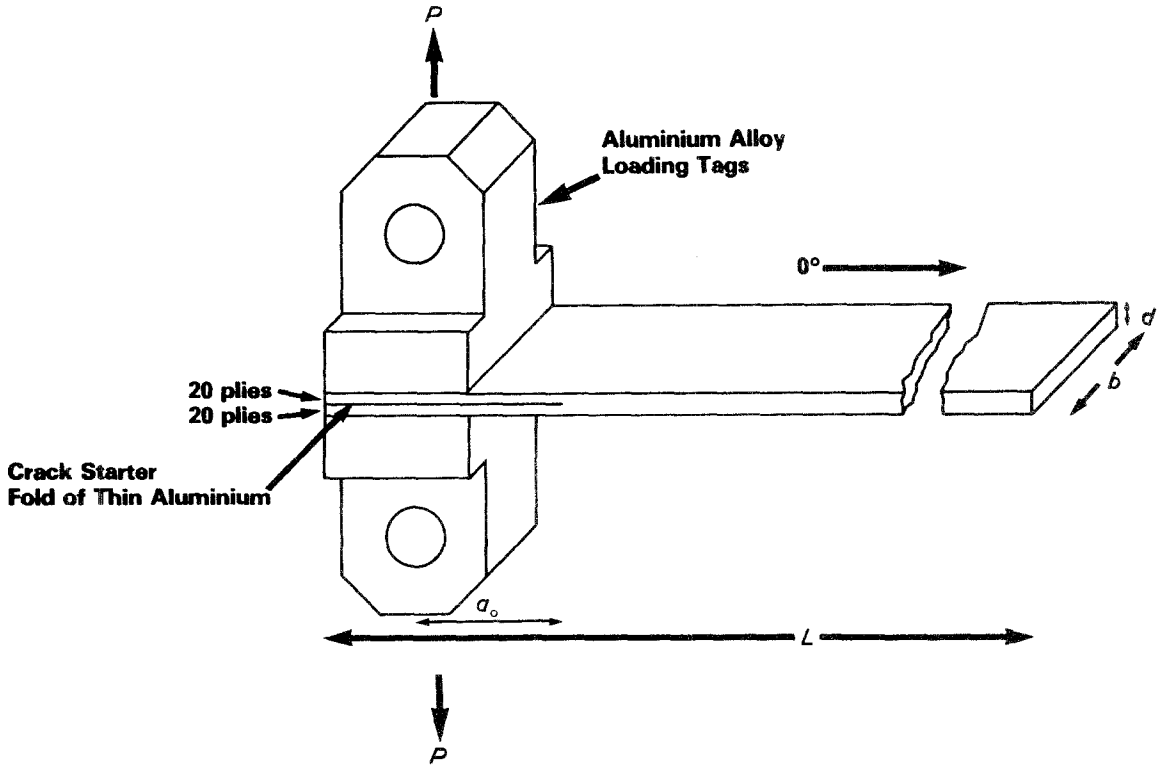

Figure 1 Double cantilever beam test arrangement. L, d and b are length, depth and width, respectively, P is force and a_0 is initial crack length.

manner with the fracture toughness measurements to provide improved insight into the interlaminar fracture processes.

2. Experimental procedure

2.1. Materials

The material used in the work was Aromatic Polymer Composite APC-2. This material consists of a matrix of Poly(ether–ether–ketone) reinforced with 61 vol % of continuous, unidirectional carbon fibres. The impregnated tape had a nominal thickness of 130 μm. The tape was moulded into laminates using a compression moulding technique with a recommended processing cycle [15]. The panels were unidirectional 40-ply laminates ($[0]_{40}$) and a crack starter, consisting of a thin fold of aluminium, was moulded between the centre plies along one edge. The quality of the panels was checked using ultrasonic C-scan.

2.2. Mechanical testing

The double cantilever beam (DCB) test was used to assess the interlaminar fracture toughness of the material. The technique is described in more detail elsewhere [9] and a summary is included here.

Parallel sided beams, 25 mm wide, were cut from the panels with the crack starter extending 30 mm into a beam from one end. Aluminium alloy end tags were bonded to the beam for the application of a load, as illustrated in Fig. 1. During testing the interlaminar crack was propagated along the complete length of the beam.

Two methods were used for analysing interlaminar fracture toughness: an 'area method' and a 'compliance method' [12]. In both cases there are some reservations as to the validity of the analysis and these have been discussed [9].

APC-2 shows two types of fracture behaviour in the DCB test. Regions of slow, stable fracture and fast, unstable fracture occur within a single beam. It is possible and helpful to analyse the toughness in the two regions separately.

2.3. Microscopy

The DCB fracture surfaces have been examined directly, after mounting and gold coating, in a JEOL T200 scanning electron microscope (SEM). This technique was used to assess the deformation and fibre damage in regions of stable and unstable crack growth. Attempts have been made to quantify the extent of fibre damage by counting broken fibre ends.

Cross-sections through the thickness of the beam, both at right angles and parallel to the fibre direction, have been prepared by embedding the sample in an acrylic embedding medium to protect the fracture surface, and then cutting it with a diamond saw. The cut cross-section was subsequently polished to a mirror finish using standard polishing techniques. Examination of the polished surface by reflected light microscopy allowed an assessment of the fracture surface profile and its relationship to features such as fibre packing and the laminar structure of the composite. The length of the fracture surface profile has been measured using a Hewlett-Packard digitizing pad and computer.

Attempts to make a more detailed study of the polished surfaces using SEM were unsuccessful because of the limited topographical features. This problem was overcome by chemically etching the surfaces using the technique of permanganic etching which was originally developed for studying the crystalline texture in polyolefines [16–21]. A recent variant of the method has been established for PEEK [22] and this has been adapted for use with APC-2. The etching process removes about a 1 μm layer of PEEK,

TABLE I Experimental results from the double cantilever beam test for APC-2

Crack propagation mode	Proportion of fracture area (%)	Number of experiment measurements	Interlaminar fracture toughness G_{IC} (kJ m^{-2})	
			Area method	Compliance method
Stable	36	39	Propagation: 2.89 (0.10)	Initiation: 2.49 (0.07)
Unstable	64	30	Propagation: 2.41 (0.11)	Initiation: 3.07 (0.14) Arrest: 1.76 (0.11)

Standard deviations of the mean value in parentheses (6 beams tested).

preferentially etching the amorphous regions and leaving the crystalline regions highlighted on the surface. Carbon fibres are unaffected by etching and are left protruding from the surface. The fracture surface remains protected by the acrylic embedding medium which is subsequently removed by dissolving it in chloroform. Considerable care was necessary throughout the preparation procedure to protect the edge between the fracture surface and the cross-sectioned surface. Finally, examination of these polished and etched specimens by SEM allowed a detailed study of the relationship between the fracture surface morphology, the sub-fracture surface morphology and the bulk morphology.

The crystallinity of the PEEK matrix was measured by X-ray diffraction [23].

3. Results

3.1. Fracture toughness results

The results from the DCB tests have been presented elsewhere [9] but a summary is included here. APC-2 shows both stable and unstable fracture in the DCB test, and although there is no pattern to this behaviour there is a tendency for more stable crack growth in the early part of the test and more unstable growth in the latter part of the test. In the six beams tested, approximately 36% of the fracture area was stable failure. The experimental results are presented in Table I.

In the area method the energy absorbed by the specimen is determined by the area under the load–deflection curve. Fracture toughness is this energy divided by the new surface area created during crack propagation. Therefore the area method gives an average propagation toughness over the new fracture area. In contrast the compliance method assumes the applicability of beam theory, and the force at a given crack length is used to calculate the toughness. Hence the compliance method gives a specific value of toughness instead of an average value. The assumptions of linear beam theory in the compliance method are known not to be rigorous as the load–deflection curves are not linear to failure. In addition there is a rotation of the specimen at the crack tip. Nevertheless, the compliance method is valuable because it can be related to specific parts of the fracture process such as initiation and arrest, particularly for unstable fracture. The area method can be used to obtain average values for the propagation process for both stable and unstable fracture.

The arrest toughness represents a minimum toughness for the material and it can be seen from Table I that the average arrest toughness is 1.76 kJ m^{-2}.

3.2. Microscopy results

Inspection of the DCB fracture surfaces by eye reveals that the regions of stable (slow) crack growth are lighter than those corresponding to unstable (fast) growth. Closer examination using SEM, shows that the level of plastic deformation is higher in the stable growth regions (Fig. 2). The micrographs were recorded from areas approximately 40 and 140 mm from the end of the fold of aluminium foil for the stable and unstable growth regions, respectively. Light scattering from the microscopic surface texture would account for the difference in appearance. In addition, Fig. 2d shows regions of plastically deformed material radiating from central points in the form of 'rosette' patterns. It will be shown that these 'rosette' patterns relate closely to the spherulitic texture of the PEEK. There is also evidence for these structures on the fracture surface produced during stable growth although they are more difficult to identify because of the greater plastic deformation. It is evident from Figs 2a and c that there is extensive fibre damage in both regions. A count of broken fibre ends reveals a larger number during stable crack growth (106 broken fibres mm^{-2}) than for unstable crack growth (77 broken fibres mm^{-2}).

Fig. 3 shows low magnification scanning electron micrographs of polished and etched cross-sections taken from both stable and unstable regions. Although in some cases the original pre-preg layers (130 μm thick) can be identified, the laminar origin of the composite is not well preserved. The plies have merged together and it is apparent that there is no continuous resin rich layer between the plies. Inclusion of a fold of aluminium foil during moulding ensures that the crack initiates as an interlaminar crack. However, it is evident from Fig. 3 that the crack rapidly deviates to become an 'intra-laminar' crack. In general, the crack favours regions of high fibre packing and this is more readily apparent for unstable crack growth. In both the stable and unstable regions, the fracture surface profile is not flat and there are many loose fibres and fibre bundles. Measurements of the lengths of the fracture surface profiles (on a scale 10 times the fibre diameter) shows that the assumed flat areas need to be increased by factors of 1.40 and 1.55 for stable and unstable growth, respectively. The higher number for

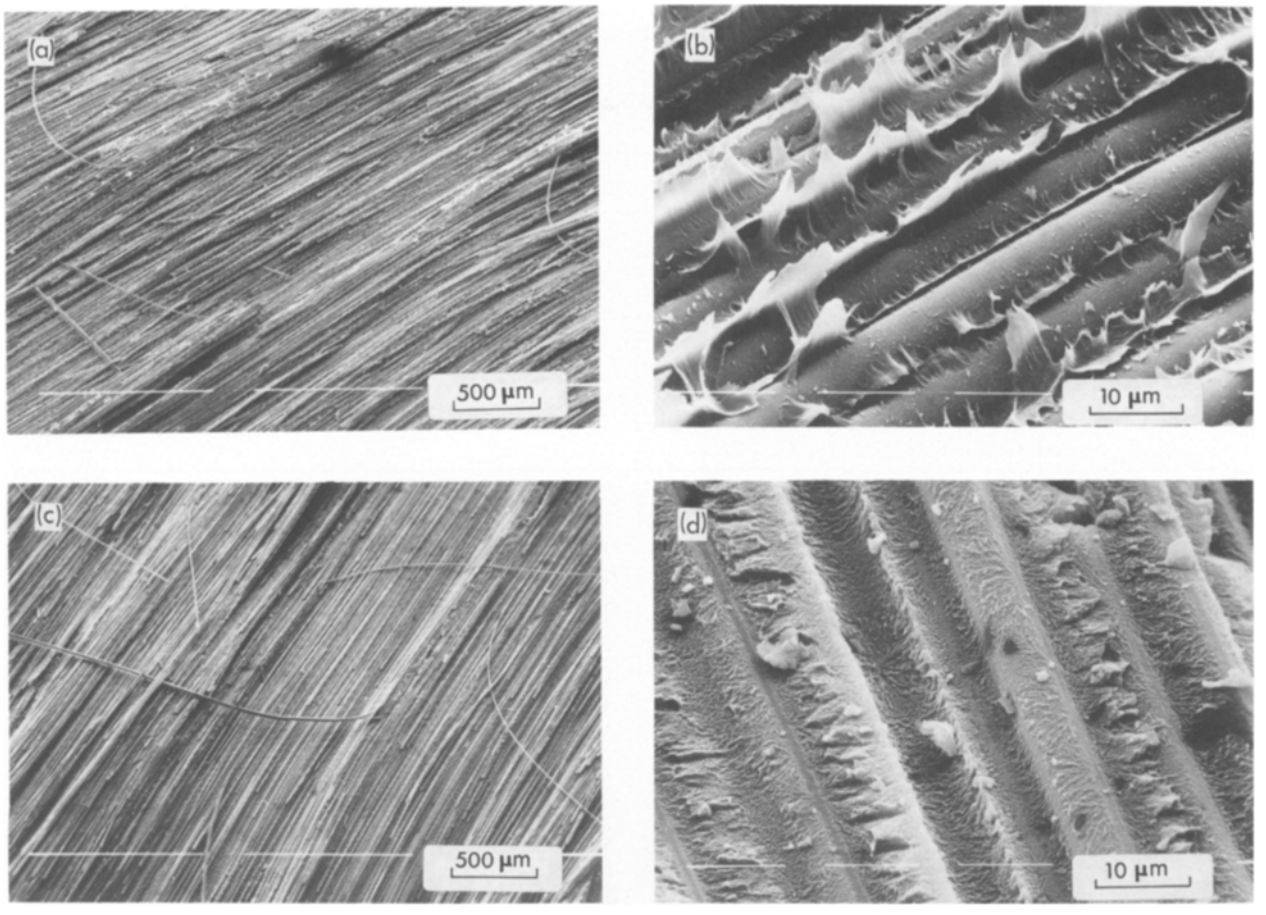

Figure 2 Scanning electron micrographs of the DCB fracture surfaces. (a) and (b) Stable crack growth; (c) and (d) unstable crack growth.

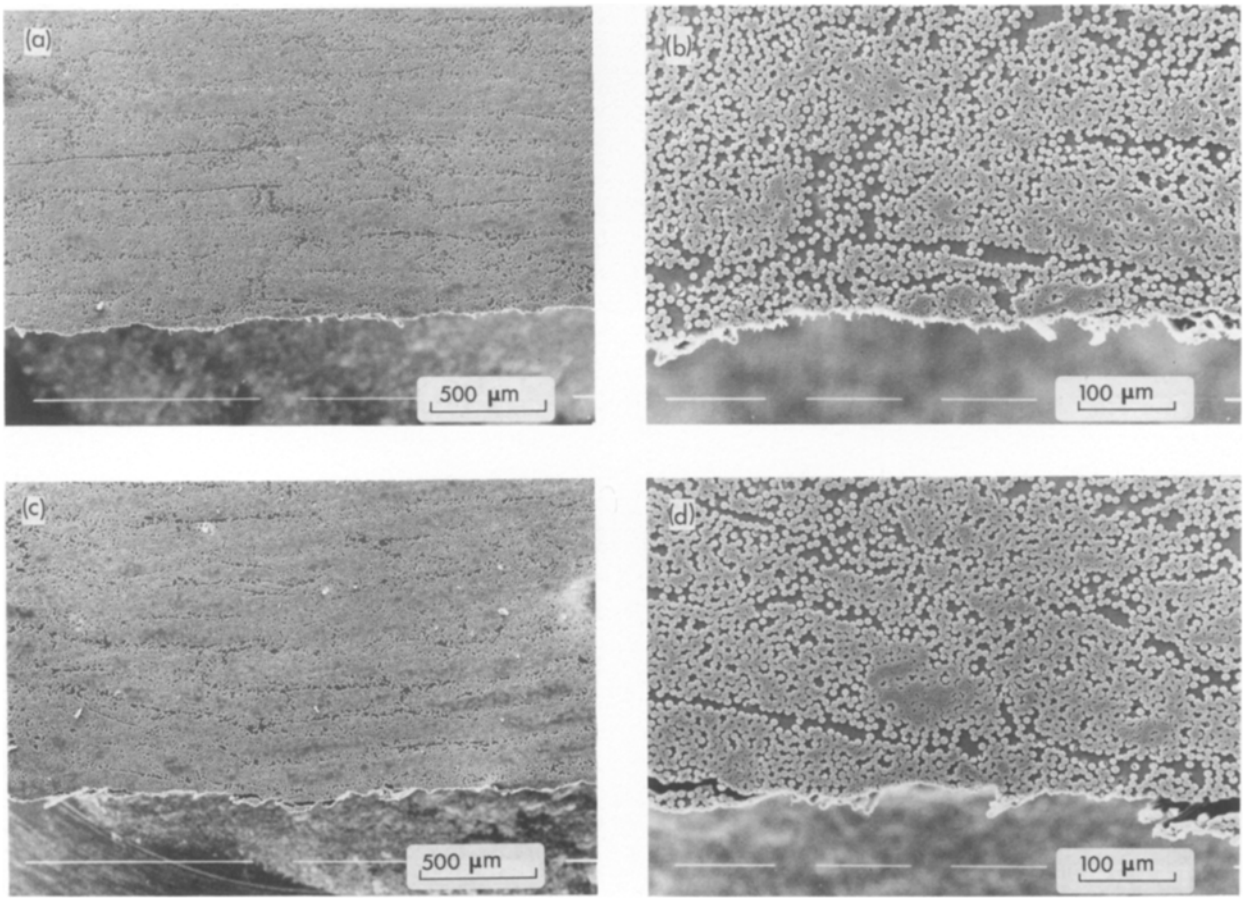

Figure 3 Scanning electron micrographs of polished and etched cross-sections through the DCB sample. (a) and (b) Close to the stable crack growth surface; (c) and (d) close to the unstable crack growth surface.

TABLE II Fibre and fracture surface properties

Symbol	Property	Stable (slow) fracture	Unstable (fast) fracture
n	Number of broken fibres per unit (fibres mm^{-2})	106	77
f_s	Surface roughness factor (dimensionless)	1.13	1.08
f_b	Detached fibre bundle factor (dimensionless)	0.27	0.47
$(f_s + f_b)$	Total area factor (dimensionless)	1.40	1.55
σ	Carbon fibre fracture strength ($MN\,m^{-2}$)	3590	
ε	Carbon fibre fracture strain (dimensionless)	0.0153	
r	Carbon fibre radius (μm)	3.5	

unstable growth is, in part, accounted for by the higher incidence of detached fibre bundles in this region. There are bridged fibre bundles which have peeled away from the fracture surface, but mainly without subsequent fibre breakage. The various contributions to increase in area for these processes are summarized in Table II.

Fig. 4 shows a higher magnification scanning electron micrograph of a polished and etched cross-section taken from the bulk of the composite, well away from the fracture surface. The PEEK matrix is about 25% crystalline and the resulting spherulitic texture is clearly evident. Nucleation of the PEEK has taken place predominantly at the fibre surfaces with the majority of nuclei occurring at the points where fibres touch or come close together. This implies a stress induced nucleation mechanism. Although shear nucleation is a possible mechanism, it is more likely that it is caused by stresses induced in the PEEK at the fibre surface as a result of differential thermal contraction during cooling. Occasionally, a spherulite is nucleated in the PEEK matrix away from the fibres but this usually occurs in matrix rich regions. It is concluded that nucleation at the fibre surface occurs at a higher temperature than in the bulk of the matrix, and that the fibre packing will influence the crystalline texture of the material. There is no evidence for a strong nucleation effect from the fibre surface which gives the trans-crystalline growth observed in some semicrystalline polymers [24]. Fig. 4 also shows artefacts of the etching process. These are manifest as small gaps between the fibres and the PEEK matrix, and occasional cracks in the PEEK between fibres that are close togehter. These are absent on the unetched, polished surfaces, and do not appear during other etching procedures such as RF plasma etching. Fig. 2 has shown the excellent wetting and adhesion of carbon fibres and PEEK. The cause of the preferential etching at the fibre surfaces is unclear.

Fig. 5 shows scanning electron micrographs of the polished and etched surfaces at the intersection with the fracture surface. The most striking feature of these micrographs, in comparison with Fig. 4, is the appearance of numerous fine cracks running approximately parallel to the fracture surface for the stable growth region. This is illustrated in more detail in Fig. 6 where the cracked region extends about 100 μm into the bulk of the composite, but the density of cracks decreases with increasing distance from the fracture surface. Similar cracks appear beneath the fracture surface for unstable growth but are confined to an ill-defined surface layer a few μm thick. Observation of polished and etched cross-sections parallel to the fibre direction reveals that the plane of the sub-surface cracks is essentially parallel to the fracture surface.

There is no evidence for these cracks on the polished surfaces before etching. It can be concluded either that the cracks were originally too fine to resolve or

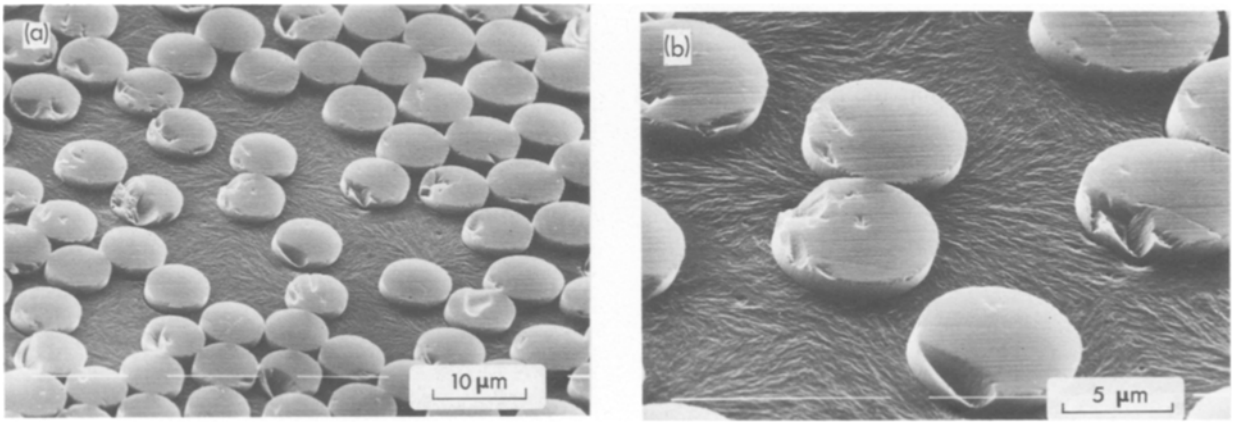

Figure 4 Scanning electron micrograph of a polished and etched cross-section showing the spherulitic texture in the bulk of the composite. (b) Enlargement of a portion of (a).

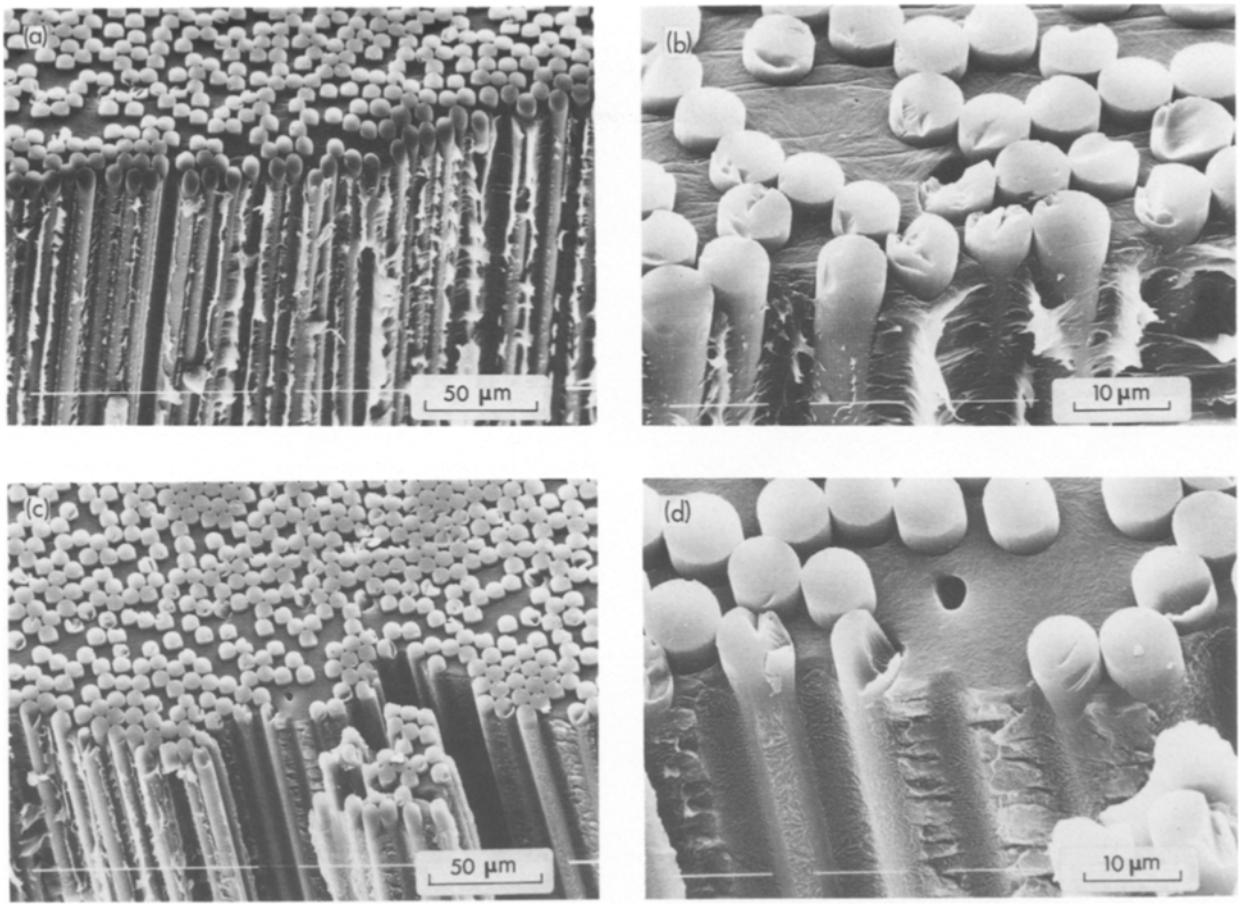

Figure 5 Scanning electron micrographs showing the intersection of a polished and etched cross-sectional surface with the fracture surface. (a) and (b) Stable crack growth; (c) and (d) unstable crack growth.

alternatively that they were not cracks but crazes or shear bands. Clearly, they correspond to failure in the material created during the fracture process which can be preferentially penetrated by the etchant. Further work is required to clarify the origin of these features. From Fig. 5 it is evident that the route of the fracture through the material has not been significantly influenced by the spherulites. It does not follow spherulite boundaries and, in general, seems to have followed a path close to the fibres and through fibre dense regions. Whilst it is to be expected that the crack will favour a route through closely packed fibres because of the higher constraint on the matrix, it should be noted that the small gaps between fibres in these areas will encourage nucleation of spherulites. Consequently there will be a degree of orientation of the lamellar crystals which may also enhance cracking.

It is clear from Fig. 5 that the acrylic embedding medium has been highly effective in protecting the fracture surface during the various stages of specimen preparation. There has been some etching at the interface but it is minimal. It is possible to gain the impression from Fig. 5 that the patterns of micro-ductility on the fracture surface do in fact relate to the radiating fine structure of spherulites. A better illustration of this observation is given in Fig. 7. Here the etched surface in the lower half of the micrograph is at 45° to the fracture surface; the broken line indicates the boundary between the two surfaces. A spherulite has been nucleated at or close to the surface of a fibre at a point N. The fibre has been removed during fracture leaving a cylindrical hollow on the fracture surface. It can be seen that there is texture on both surfaces radiating from the point N. On the etched surface the texture relates to bundles of lamellar crystals and on the fracture surface closer examination reveals that it is micro-ductility. It is clear that the texture on both surfaces has a common origin, and that the crystallinity and crystal morphology will have a significant effect on micro-deformation. It is suggested that the numerous 'rosette' patterns of micro-plasticity seen particularly on the fracture surface in the unstable growth regions are caused by spherulites.

4. Fracture energy contributions

It is apparent from the previous section that there are a large number of different failure processes contributing to the interlaminar fracture. These include fracture of the polymer (which includes sub-surface effects), fibre peeling and fibre fracture, and the situation is further complicated by the fact that the fracture surface is not perfectly planar. In order to understand the interlaminar fracture further it is useful to estimate the energy contributions from these various processes, and in particular to calculate the energy associated with polymer fracture. The calculations will be approximate because of the need for a number of simplifying assumptions, as detailed in the following sections.

Prior to considering the quantitative analysis of the energy absorption processes it is helpful to consider

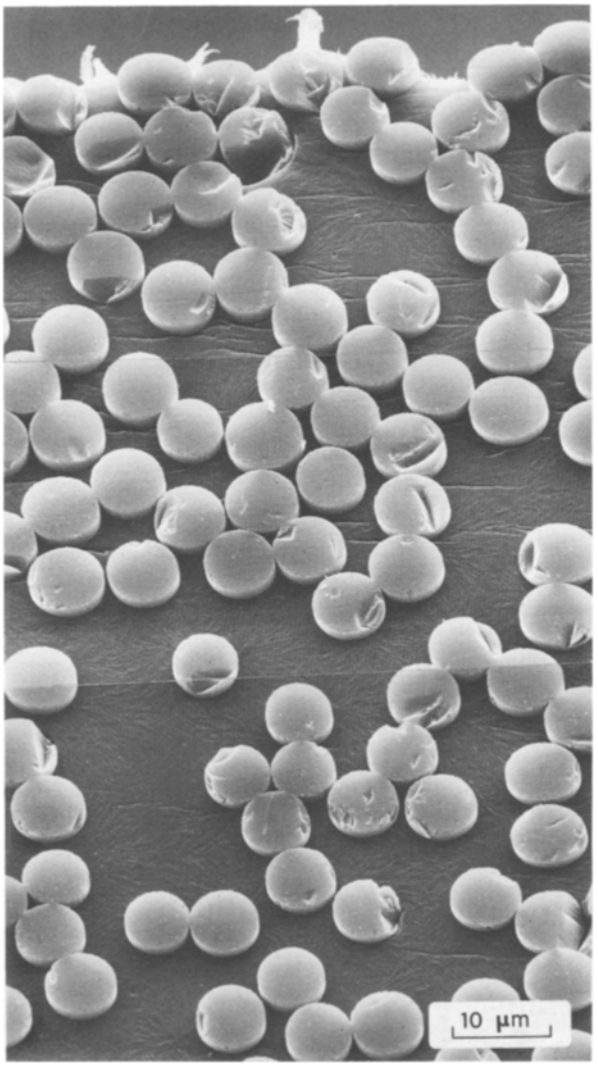

Figure 6 Scanning electron micrograph of a polished and etched cross-section showing sub-surface "cracks" close to the stable fracture surface.

the sequence of events. The interlaminar crack proceeds through the polymer. During this process the crack front meets misaligned fibres, resulting in fibres bridging the gap. Further crack propagation results in these fibres being peeled from the surface. Individual fibres will break whereas bundles will peel over longer distances. Many of these bundles remain intact and therefore peel over the length of the beam. These processes and features are illustrated in Fig. 8.

The total energy involved in fracture will be the sum of the individual contributions

$$U_C = U_P + U_R + U_F + U_O \quad (1)$$

where U_C = composite fracture energy; U_P = polymer fracture energy; U_R = peeling energy; U_F = fibre fracture energy, and U_O = other unknown contributions. It will be assumed that U_O is negligible. In addition, if energy per unit area (γ) for a specific process is considered and where $\gamma_c = (G_c)_{exp}$, then it is possible to relate the measured fracture toughness $[(G_c)_{exp}]$ to the various energy contributions.

It is known, however, that the fracture surface is non-planar. Consequently, instead of the surface area being unity, it will be f_s (where $f_s \geqslant 1$ as discussed in Section 3). The interlaminar cracks start to propagate

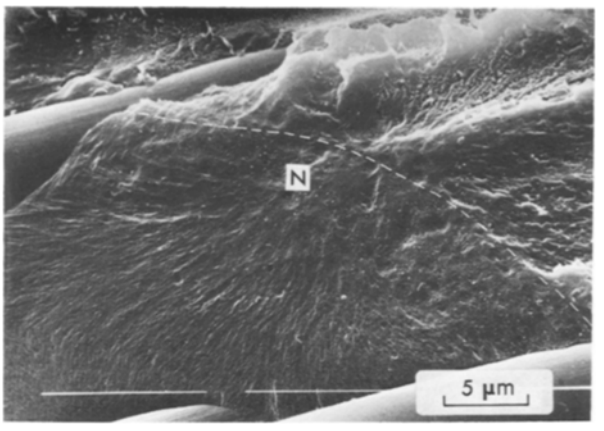

Figure 7 Scanning electron micrograph from the intersection of a cross-sectional surface with the fracture surface for the unstable growth region showing texture on both surfaces which relates to a spherulite nucleated at the point N.

through the matrix and subsequently may invoke other mechanisms of fracture (e.g. fibre peeling, fibre breakage). Account is taken of the fracture surface roughness by modifying to the polymer energy term, which becomes $f_s\gamma_P$.

Therefore

$$(G_c)_{exp} = f_s\gamma_P + \gamma_R + \gamma_F \quad (2)$$

where γ_P = polymer fracture energy/unit area; γ_R = peeling energy/unit area; γ_F = fibre fracture energy/unit area; f_s = surface roughness factor (Table II), and $(G_c)_{exp}$ = experimental fracture toughness. Because the energy associated with polymer fracture is required then Equation 2 is re-arranged.

$$\gamma_P = \frac{1}{f_s}[(G_c)_{exp} - \gamma_R - \gamma_F] \quad (3)$$

The contribution to peeling is in two parts; individual fibres which break and bundles which remain intact. For those fibres which peel over short distances and break, it is assumed that, on average, half the surface of a fibre is involved in the peeling and that the layer of polymer adhering to the fibre is relatively thin.

For n broken fibres per unit area with average detachment length $\bar{l}$, the peel area is $\pi r\bar{l}n$. In addition it is assumed that the polymer fracture energy in peeling and in crack propagation are the same, which seems reasonable as the processes occur at the same rate. Therefore this peel energy per unit area is

$$\gamma_{R_1} = \gamma_P n\bar{l}\pi r \quad (4)$$

The second contribution to peel energy is that for unbroken fibre bundles. This provides an energy contribution of

$$\gamma_{R_2} = \gamma_P f_b \quad (5)$$

where f_b is the area factor given in Table II due to detached fibre bundles, and as explained in Section 3.

The total peel energy per unit area is

$$\gamma_R = \gamma_{R_1} + \gamma_{R_2} \quad (6)$$

Therefore

$$\gamma_R = \gamma_P(n\bar{l}\pi r + f_b) \quad (7)$$

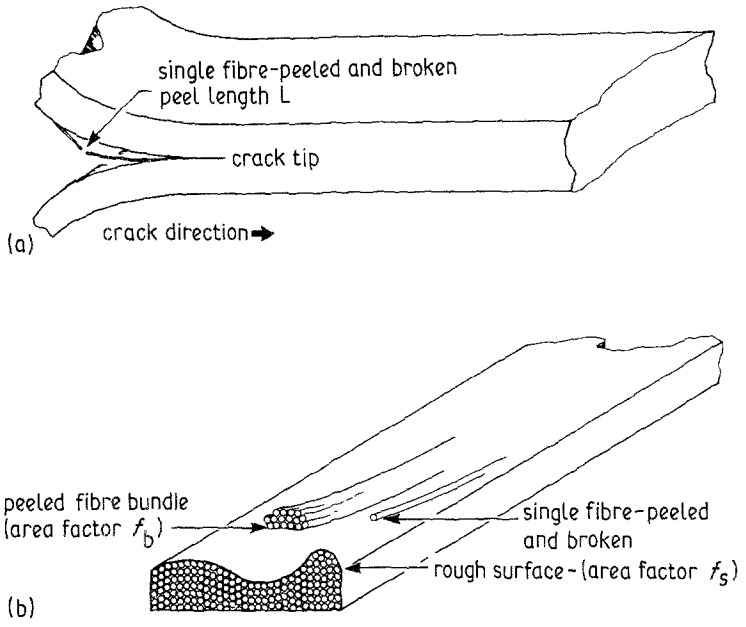

Figure 8 Schematic diagram of the DCB sample showing (a) a peeled and broken fibre, and (b) a peeled fibre bundle and the rough fracture surface.

The next energy contribution to consider is that due to fibre fracture (γ_F). The energy involved can be determined from a tensile test on aligned fibres. On the basis of elastic behaviour to fracture, the area encompassed by the force–deflection ($F - \delta$) characteristic would equate to the fracture energy (i.e. $\frac{1}{2}F\delta$). This can be expressed in terms of measured values of fibre fracture stress (σ) and strain (ε) with a knowledge of fibre radius (r) and a mean gauge length of fibres at fracture, which we assume is the detachment length ($\bar{l}$). For n broken fibres per unit area, the fibre fracture energy per unit area can thus be expressed

$$\gamma_F = \tfrac{1}{2}\sigma\varepsilon\pi r^2\bar{l}n \tag{8}$$

Combining Equations 3, 7 and 8 gives

$$\gamma_P = \frac{1}{f_s}[(G_c)_{exp} - \gamma_P(n\bar{l}\pi r + f_b) - \tfrac{1}{2}\sigma\varepsilon\pi r^2\bar{l}n] \tag{9}$$

Combining terms in γ_P gives

$$\gamma_P = \left[\frac{(G_c)_{exp} - \frac{1}{2}\sigma\varepsilon\pi r^2\bar{l}n}{f_s + n\bar{l}\pi r + f_b}\right] \tag{10}$$

The relevant fibre and fracture surface properties necessary to conduct calculations are summarized in Table II.

The only remaining unknown in Equation 10 is the mean detachment length involved in fibre fracture ($\bar{l}$). It is estimated from the micrographs that this length is 0.5 mm but the effects of other lengths have also been considered.

Table III summarizes the calculations of energy per unit area for polymer fracture, fibre peeling and fibre fracture. In these calculations the value for $(G_c)_{exp}$ for stable (slow) fracture is obtained from the area method (see Table I) and the value for unstable (fast) fracture is the arrest value from the compliance method calculations.

With reference to the summaries in Table III, and assuming that the estimated fibre detachment length of 0.5 mm is correct then a number of conclusions emerge for stable and unstable fracture. In both cases, the polymer process absorbs the most energy; 56% for stable fracture, 52% for unstable fracture. The fibre breakage process absorbs least energy, only 2% in both cases. The peeling process is intermediate, but with different contributions from broken single fibres and detached bundles according to crack speed (i.e. stable and unstable fractures). For stable fracture, 42% of the energy contribution is due to peeling, compared with 46% for unstable fracture. However, for stable fracture the 42% is made up of 29% due to single broken fibres with only 13% due to bundle detachment. For unstable fracture the 46% comprises 21% due to broken single fibres and a bundle detachment contribution of 23%.

It is also useful to relate the calculated polymer fracture energies to the deformation regions shown in Figs 5 and 6. In order to calculate these energies it is necessary to use analytical expressions. These are available from linear elastic fracture mechanics theory, and these will be applied here despite their obvious limitations.

The plastic zone size (r_p) depends on whether plane strain or plane stress conditions are prevalent. For plane stress conditions

$$r_p = \frac{1}{2\pi}\left(\frac{K_c}{\sigma_y}\right)^2 \tag{11}$$

For plane strain conditions

$$r_p = \frac{1}{6\pi}\left(\frac{K_c}{\sigma_Y}\right)^2 \tag{12}$$

where K_c = critical stress field intensity factor for the polymer, and σ_Y = yield stress for the polymer. K_c can be calculated using the expression

$$K_c = (G_cE)^{1/2} \tag{13}$$

where G_c = critical strain energy release rate for the polymer, and E = a modulus for the polymer.

In order to determine K_c using Equation 13, it is assumed that γ_p can be equated to G_c and that an appropriate polymer modulus is 3.5 GN m^{-2} (this modulus relates to 100 sec under load at 23° C at small strains).

TABLE III Calculated fracture energy contributions in interlaminar fracture

Fracture mode	Experimental G_c (kJ m^{-2})	Mean fibre detachment length (mm)	Fracture energy contributions (kJ m^{-2})			
			Polymer γ_p	Peeling γ_{R_1}	γ_{R_2}	Fibre breakage γ_F
				Single fibres	Detached bundles	
Stable	2.89*	0.2	1.76	0.41	0.48	0.02
		0.5‡	1.43	0.83	0.39	0.06
		1.0	1.08	1.26	0.29	0.11
Unstable	1.76†	0.2	1.03	0.15	0.48	0.02
		0.5‡	0.87	0.37	0.41	0.04
		1.0	0.70	0.59	0.33	0.08

*Area method analysis.
†Compliance method analysis at arrest.
‡Estimated detachment length from micrographs.
From Equation 2, $(G_c)_{exp} = f_s\gamma_p + (\gamma_{R_1} + \gamma_{R_2}) + \gamma_F$.

Values of γ_P ($\bar{l} = 0.5$ mm) from Table III are available for stable and unstable fractures. Therefore

$$(K_c)_{STABLE} = 2.24\,MN\,m^{-3/2}$$

$$(K_c)_{UNSTABLE} = 1.74\,MN\,m^{-3/2}$$

The yield stress of PEEK at 23° C is 95 MN m^{-2} and using this value together with the values for K_c stable and unstable, enables plastic zone sizes to be determined from Equations 11 and 12. Observations of the fracture morphology strongly suggest that stable crack growth produces plane stress conditions for fracture of the matrix. Therefore Equation 11 provides a value for the plastic zone

$$(r_p)_{STABLE} = 88\,\mu m$$

For unstable fracture, the morphological evidence suggests that the polymer fracture relates to plane strain conditions. Therefore Equation 12 is used to determine the plastic zone size.

$$(r_p)_{UNSTABLE} = 18\,\mu m$$

A plastic zone is equated to a deformation zone in the composite.

Fig. 6 shows that in the region of stable fracture the deformation zone extends approximately 100 μm into the bulk of the composite; the calculated value is 88 μm. In the unstable region the deformation zone size is observed to be approximately 7 μm and the calculated value is 18 μm. This agreement is at least encouraging, in view of the oversimplifications necessary in the argument.

5. Discussion

5.1. Fracture surface morphology

Double cantilever beam fracture surfaces of composite specimens show many features in addition to matrix failure. These include merging of adjacent plies preventing a planar interlaminar region, fibre bridging (peeling of fibres from the fracture surface) and fibre breakage.

In this work an attempt is made to quantify these various failure processes, whilst previous work has often been qualitative. It is observed that there are differences in both the number of broken fibres per unit area and the amount of surface roughness between the stable and unstable fracture regions. In the stable region the fracture energy of the polymer is higher than in the unstable region (Table III). The peeling process (which involves polymer fracture) requires less energy in the unstable region and hence detached fibres are more likely to be peeled from the surface rather than broken. However in the stable region the peeling will involve greater energy and so it is more likely that a detached fibre will break rather than being peeled. Therefore the observed differences in the numbers of broken fibres can be explained from a knowledge of the fracture energy contributions. This underlines the need for a quantitative approach to fracture morphology in order to understand the interlaminar fracture process.

There is a concern that the presence of spherulites may lead to weakness as the fracture path may follow spherulite boundaries or axes. The evidence from this study is that the spherulite boundaries have no effect on the fracture path, with the crack passing randomly through spherulites.

It has been shown (Fig. 7) that the 'rosette' patterns of microductility on the fracture surface relate to the microstructure of spherulites. These patterns are more apparent in the unstable fracture regions. In the stable regions, the polymer fracture is dominated by the plastic deformation in the hollows between the fibres.

5.2. Fracture energy contributions

The quantitative approach to the microscopy has enabled a calculation of the fracture energy contributions. Whilst there are a number of assumptions, the general approach is useful in separating out the contributions from the different processes. A number of points emerge from the values in Table III. The values depend on the gauge length of the detached fibres and therefore these must be known with some confidence. Our observations indicate that the typical length is 0.5 mm, however Table III enables the effect of the gauge length to be taken into account. For the range of gauge lengths examined the fracture energy contribution from fibre breakage is relatively small. In the largest case it represents less than 10% of the experimentally measured toughness and hence fibre

breakage does not make a significant contribution to the measured toughness.

There is a significant contribution from the peeling process, up to 50%. This is due to polymer failure and is expected to be typical of interlaminar fracture processes. The resin rich interlaminar layer in APC-2 is thin and therefore ply merging, which is likely to be the major cause of peeling, will be common.

It is possible that in the interlaminar fracture of some lay ups of APC-2 the peeling and fibre breakage processes will not occur. Consequently fracture will be solely planar within the matrix. In this case the interlaminar toughness would be equal to the polymer fracture energy contribution of Table III. It can be seen that with the typical fibre gauge length of 0.5 mm the polymer fracture energy is $840\,J\,m^{-2}$ for the unstable fracture and $1350\,J\,m^{-2}$ in the stable fracture. The unstable value is based on a toughness measured at arrest and therefore represents a minimum for the material. This value of $840\,J\,m^{-2}$ is considerably higher than the experimentally measured toughness on most high performance composite systems [25], which will in any case include unknown contributions from the other failure mechanisms.

5.3. Deformation zones

An important feature to emerge from the microscopy is the presence of zones of deformed polymer which extend into the bulk of the material from the fracture surface. These represent permanent deformation of the polymer and therefore a contribution to the energy absorbed in interlaminar fracture.

One of the limitations of high performance composites is their poor resistance to delamination, characterized by low interlaminar fracture toughness. Polymers with increased toughness have been used in an attempt to improve composite interlaminar toughness, but this has not led to proportionate increases in composite toughness [26]. A relationship between resin toughness and composite toughness has been discussed by Hunston [25].

For resins with low toughness, the composite toughness exceeds or equals that of the resin. In this case the plastic zone size will be smallest and less than the thickness of the interlaminar region. Hence the full resin deformation processes are developed in the composite. Fibre bridging, fibre breakage and merging of plies will give additional contributions to the composite toughness. Consequently, low toughness resins produce higher toughness composites. However, for resins with $G_c > 50\,J\,m^{-2}$ the composite toughness does not increase in direct proportion with resin toughness. This is attributed to the fact that the fibres constrain the matrix and hence a full plastic zone cannot develop in the interlaminar region [26]. Various calculations to determine the resin toughness at which the plastic zone size equals the interlaminar thickness at the point at which composite toughness becomes less than resin toughness show good agreement with experimental results [25, 27]. Recently a model has been proposed in which the plastic zone size extends beyond the interlaminar region [28].

It is commonly believed that the region of deformation is contained in the interlaminar region. It is clear from Fig. 5 that cracks are not confined to the interlaminar region and that the deformation zone exceeds the interfibre distance. The use of a thick interlaminar layer to increase toughness is therefore unnecessary for materials which can develop these relatively large deformation zones. Any consequential penalty relating to a lower attainable fibre volume is not incurred.

A pre-requisite to the development of a deformation zone is that the interface between the fibre and the matrix must be good in order to ensure that the stresses are transferred back into the bulk of the composite. In APC-2 the interface is clearly sufficiently strong, and no bare fibres are evident on the fracture surface. The combination of the good interface combined with the tough and ductile polymer lead to a large volume of resin being brought into the failure process which leads to the high interlaminar fracture toughness observed in both stable and unstable fracture.

6. Conclusions

A number of failure processes are seen to occur in interlaminar fracture. These include fibre breakage, fibre peeling and polymer fracture, and additionally the fracture surface is not planar but has surface roughness. The extent of polymer ductility differs in the stable and unstable fracture regions, as do surface roughness and extent of fibre breakage. The quantitative approach to the microscopy enables the energy contributions from these various fracture processes to be estimated. The polymer fracture energy is at least 44% of measured toughness, whereas the contribution from fibre fracture is less than 10%.

The use of an etching technique enables the spherulite texture to be revealed and spherulites are seen to nucleate from the fibre surfaces predominantly at the point of contact of fibres. Patterns of microductility on the fracture surfaces are seen to be due to the spherulite texture, however the spherulite boundaries do not influence the fracture path.

Deformation zones consisting of fine cracks are seen to extend into the bulk of the composite from the fracture surface. The deformation zone extends approximately $100\,\mu m$ into the composite in stable fracture and $7\,\mu m$ in unstable fracture. The size of the plastic zone has been calculated using the polymer fracture energies and fracture mechanics concepts. There is reasonable agreement between the calculated and observed deformation zone sizes. The nature of the deformation zone remains uncertain but cracking, crazing or shear banding mechanisms are postulated. Nevertheless the presence and size of the deformation zone indicates that the volume of polymer in which energy can be absorbed extends considerably beyond interfibre or interlaminar distances.

This conclusion challenges current theories for predicting composite toughness from resin toughness data. It would appear that the improved ductility available with thermoplastics will require modification to the toughness rules for composites.

References

1. F. N. COGSWELL and D. C. LEACH, *Plastics and Rubber Processing and Application* **4** (1984) 271.
2. G. R. BELBIN, *Inst. Mech. Eng. Proc.* **198** (1984).
3. J. B. CATTANACH and F. N. COGSWELL, in "Developments in Reinforced Plastics", Vol. 5, edited by G. Pritchard (Applied Science Publishers, 1985).
4. N. J. JOHNSTON, in Proceedings of the ACEE Composite Structures Technology Conference, Seattle, August 1984.
5. J. T. HARTNESS, *National SAMPE Symposium* **29** (1984) 459.
6. G. DOREY, S. M. BISHOP and P. T. CURTIS, in Proceedings of a Conference on Composites: Materials and Engineering, University of Delaware, September 1984.
7. D. R. CARLILE and D. C. LEACH, in Proceedings of the 15th National SAMPE Technical Conference, Vol. 15 (1983) p. 82.
8. D. C. LEACH and D. R. MOORE, *Composites Science and Technology* **23** (1985) 131.
9. D. C. LEACH, D. C. CURTIS and D. R. TAMBLIN, in Proceedings of the ASTM Symposium on Toughened Composites, Houston, March 1985, to appear in ASTM Special Technical Publication.
10. C. Y. BARLOW, M. V. WARD and A. H. WINDLE, in Proceedings of the 6th Conference on Deformation, Yield and Fracture of Polymers, Churchill College, Cambridge, March 1985.
11. R. A. CRICK, D. C. LEACH, P. J. MEAKIN and D. R. MOORE, in Proceedings of the 1st European Conference on Composite Materials, Bordeaux, September 1985.
12. J. M. WHITNEY, C. E. BROWNING and W. HOOGSTEDEN, *J. Reinforced Plastics and Composites* **1** (1982) 297.
13. H. CHAI, *Composite* **15** (1984) 277.
14. W. D. BASCOM, in Proceedings of the ASTM Symposium on Toughened Composites, Houston, March 1985. To appear in ASTM Special Technical Publication.
15. Aromatic Polymer Composites APC-2 data sheets, ICI Advanced Materials Business Group.
16. R. H. OLLEY, A. M. HODGE and D. C. BASSETT, *J. Polym. Sci. Polym. Phys. Ed.* **17** (1979) 627.
17. R. H. OLLEY and D. C. BASSETT, *Polymer* **23** (1982) 1707.
18. D. C. BASSETT and A. M. HODGE, *Proc. R. Soc.* **A359** (1978) 121.
19. *Idem, ibid.* **A377** (1981) 25.
20. *Idem, ibid.* **A377** (1981) 39.
21. *Idem, ibid.* **A377** (1981) 61.
22. D. C. BASSETT, R. H. OLLEY and D. J. BLUNDELL, unpublished results.
23. D. J. BLUNDELL, J. M. CHALMERS, M. W. McKENZIE and W. F. GASKIN, unpublished results.
24. R. H. BURTON and M. J. FOULKES, *Plastics and Rubber Processing and Application* **3** (1983) 129.
25. D. L. HUNSTON, *Composites Technology Review* **6** (4) (1984) 176.
26. W. D. BASCOM, J. L. BITNER, R. J. MOULTON and A. R. SIEBERT, *Composites* **11** (1980) 9.
27. D. L. HUNSTON, R. J. MOULTON and N. J. JOHNSTON, unpublished results.
28. W. L. BRADLEY and R. N. COHEN, in Delamination and Debonding of Materials (ASTM STP, 1985) p. 876.

Received 22 July
and accepted 22 September 1986